Adaptive Incremental Dynamic Inversion for Fault-tolerant Flight Control of a Flying Wing

Ul Haq, R.S.; Atmaca, D.; van Kampen, E.

DOI
10.2514/6.2026-1744

Publication date
2026

Document Version
Final published version

Published in
Proceedings of the AIAA SCITECH 2026 Forum

Citation (APA)
Ul Haq, R. S., Atmaca, D., & van Kampen, E. (2026). Adaptive Incremental Dynamic Inversion for Fault-tolerant Flight Control of a Flying Wing. In *Proceedings of the AIAA SCITECH 2026 Forum* Article AIAA 2026-1744 American Institute of Aeronautics and Astronautics Inc. (AIAA). https://doi.org/10.2514/6.2026-1744

AIAA SciTech Forum
12-16 January 2026, Orlando, FL
AIAA SCITECH 2026 Forum

10.2514/6.2026-1744

Adaptive Incremental Dynamic Inversion for Fault-tolerant Flight Control of a Flying Wing

Rana Husain Ali Ul Haq *, Direnc Atmaca †, and Erik-Jan van Kampen ‡
Delft University of Technology, Kluyverweg 1, 2629HS, Delft, The Netherlands

Sustainability is a key commitment for future innovation and improvement of the aerospace industry and to realise active research is invested towards advanced and new aircraft designs such as the FLYING V™. The Flying V is a flying wing design for commercial aviation, promising higher efficiency against conventional tube-and-wing aircraft. The Flight Control System (FCS) has to be designed to prove the airworthiness of the aircraft. In this work, a fault-tolerant FCS is designed that includes an adaptive incremental dynamic inversion inner loop rate control law with an outer loop that consists of longitudinal C* control law and Rate Control Attitude Hold roll control laws for lateral control. Research and activities has led to an updated geometry design with aerodynamic data from RANS simulation, which requires tuning of its outer loop flight controls to be within level 1 handling quality. To investigate the fault tolerance of the aircraft with a structural fault case that results in a loss of effectiveness. It is shown that the adaptation allows the aircraft to cope with the faults and maintain satisfactory tracking performance.

I. Introduction

The FLYING V™* is an advanced aircraft design of a Flying Wing (FW) concept researched at the Delft University of Technology. This aircraft design provides significant energy efficiency improvement for the realisation of a viable and more energy-efficient alternative to the conventional tube-and-wing design. The development of new advanced aircraft designs is a pillar of key innovations and necessary to further sustainability and improvement of the aerospace industry [1]. With the Flying V being an unconventional aircraft design, the research and development of the Flying V will result in many potential changes over time, such as from optimizations in regard to its aerodynamic design and structural design, engine placement or control surface adjustments, which will all introduce different characteristics of the aircraft. Such additions will go through testing and new data or requirements can be introduced over time as the aircraft matures from its baseline. The design and development of Flight Control System (FCS) has to be updated with these changes and is essential for the aircraft's airworthiness and compliance for certification.

Initial research towards the flying and handling qualities of the Flying V was performed with a linear aerodynamic model, estimated at a limited set of flight conditions, obtained using the Vortice Lattice Method (VLM) [2]. The VLM model was combined with wind tunnel data from Wind Tunnel Test Experiments (WTE) with a scaled Flying V model [3]. This combination was done to include the pitch break tendency at higher angle of attack that was captured with these experiments, as VLM does not capture these nonlinear phenomena. With this combined model, a study was performed to improve its handling qualities with by incorporating Incremental Nonlinear Dynamic Inversion (INDI), which is a sensor based control law that relies on an onboard Control Effectiveness (CE) model derived from aerodynamic parameters of the control surfaces, in the inner loop [4]. The implemented FCS was revised with outer loop controllers based on C* parameter for longitudinal control, roll rate command and sideslip compensation for directional control and augmented with Flight Envelope Protection (FEP) for angle of attack, load factor and roll angle protection [5]. Additionally, the FCS was tuned and evaluated to adhere to Level 1 Flying qualities with sensor dynamics. Numerical simulations revealed that the FCS is robust against aerodynamic uncertainties up to 20%, but its control effort increased with the aerodynamic uncertainty, which was especially apparent for the rudder where additional oscillations were observed due to low control authority resulting in degrading performance.
The VLM model and combined model were also used in various pilot-in-the-loop simulator studies and various

*MSc. Student, Control and Simulation, Faculty of Aerospace Engineering, r.h.a.ulhaq@student.tudelft.nl
†PhD Candidate, Control and Simulation, Faculty of Aerospace Engineer, d.atmaca@tudelft.nl
‡Associate Professor, Control and Simulation, Faculty of Aerospace Engineering, e.vankampen@tudelft.nl
*Flying V is a trademark of Fortescue, The Flying V design is owned by Fortescue, UK & NL patents pending

manoeuvres were covered [6]. The FCS with FEP and compared with other FCS has been tested in a simulator pilot experiments, which confirmed the limited control authority due to control surface saturation, which was also observed in previously conducted piloted experiments [7–9].

The Flying V's control surface layout provides redundant control effectors, which can provide control authority for pitch and roll, but limited control authority during manoeuvres could require additional pilot effort to maintain stability and in case of control surface failure, it can impede on the flight safety of the aircraft. One of the largest reasons for aircraft incidents is Loss-of-Control (LOC-I) in commercial aviation [10, 11], which has been trending downwards as Fly-by-Wire systems have become more advanced, and with further research and development towards Fault Tolerant Flight Control (FTFC) systems further reduction can be obtained. One class of FTFC design is active FTC, whereby adaptive control methods are employed to achieve reconfigurable flight control laws, which can continuously adapt its control parameters to ensure the safe operation of the aircraft by 'intelligent' and informed updates of its control effectiveness to utilise its control authority on the remaining control effectors in case of faults and thus reduce the required pilot effort [12, 13].

Adaptive INDI has seen recent advancements in the applications for drones [14], Vertical Take-off and Landing (VTOL) drones [15] and numerical simulations with an F-16 simulation model to achieve consistent handling qualities [16] and applied in [17] for fault tolerance of the Flying V. In [14] the Least Mean Squares (LMS) filter was implemented to perform online adaptation of its onboard CE model, as INDI with no adaptation had degraded performance due to CE model mismatch. In [16] CE inaccuracy due to uncertainties lead to varying handling quality and stability characteristics, which were improved through adaptation with LMS that corrected its onboard CE model. In [15] a parametric model using Multivariate B-spline to model its CE model was applied, which stored and adapt to new parameters online to identify the effectiveness. A two-step state and parameter estimation with Extended Kalman Filter (EKF) for state estimation and Recursive Least Squares (RLS) parameter estimation combined with variable forgetting factor has been applied in [17]. The adaptation of the CE model, which consists of coefficients from the aerodynamic model with respect to the dynamics in the inner loop. It was shown that the two-step parameter estimation would not determine the true estimation of its control effectiveness, but adaptation of its CE model would lead to other control surfaces compensating for the damaged control surface.

As the Flying V research is in constant development, a newer parametric geometry [18], which researched a family series of the Flying V, has been used to synthesise an aerodynamic model, for the full-scale aircraft with Reynolds-averaged Navier Stokes (RANS) simulations and VLM simulations [19].This new aerodynamic model provides more flight envelope points, determined at different angle of attacks, Mach numbers and altitudes and incorporates nonlinearities, which can estimate the occurrence of the pitch break at the various flight envelope points. Research has also been conducted towards control surface sizing and placement to satisfy certification requirements and achieve control authority for safe and operable flight [20].

The contributions of this paper are to investigate the possible performance degradation of the INDI inner rate control loop when faced with faults and use RLS to adapt the onboard CE model to cope with the fault and maintain accurate reference tracking performance. This research also uses the updated aerodynamic model and has updated the outer loop gain tuning routines.

The outline of the paper is as follows. In section II, a description of the simulation model of the Flying V is described, control surface layout (II.A), aerodynamic model & parameters (II.B), actuator model (II.C), airframe dynamics (II.D) and lastly sensor model (II.E). The FCS used in this paper is outlined in section III with a description of the outer loop controllers (III.A), the inner loop for rate control with INDI (III.B), The adaptive INDI implementation III.C), a description of how faults are injected (III.D) and lastly the tuning of outer loop controller (III.E). Finally, the simulation results are presented in Section IV, with the discussion and lastly the conclusion in Section V.

II. Flying V Simulation Model

The aircraft simulation model defines the dynamics used for this research where at first, the control surface layout, aerodynamic model and parameters used in the model are described, thereafter the actuator dynamics, formulation of the rigid-body equations of motions and lastly the sensor dynamics are defined.

A. Control Surface Layout

The control surface layout used for this simulation model considers inboard and outboard elevons located at the trailing edge of the wing ($\delta^{L/R}_{CS1}, \delta^{L/R}_{CS2}$) for the right and left sides respectively. The inner and outboard elevon can be used for pitch and roll control. A rudder ($\delta^{L/R}_{CS3}$) is integrated into the winglets on the right and left sides respectively for yaw (directional) control. The geometry of the design is shown in Figure 1, including an optimal engine distance first estimated [21] and is still under investigation. The landing gear was not taken into account for the study.

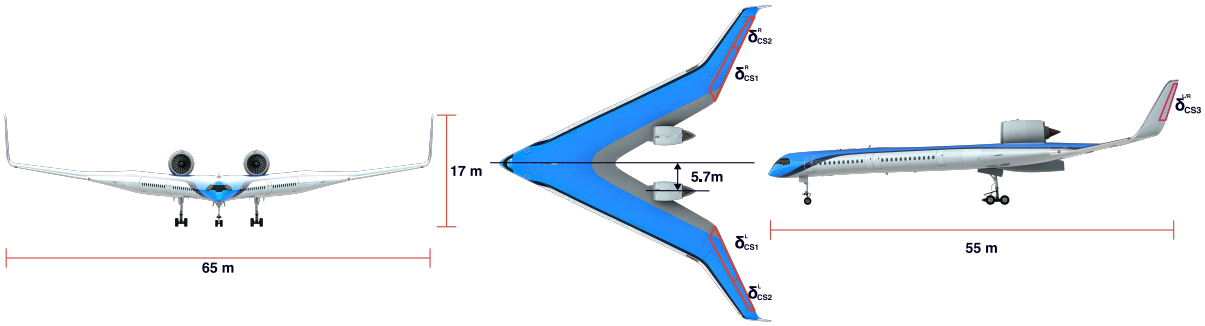

Fig. 1 Front, top and side view of the Flying V with (outer) dimensions and control surfaces

B. Aerodynamic Model & Aircraft Parameters

The aerodynamic model is from an early iteration of the study in [19], and is derived from a combination of RANS and VLM simulations at various flight envelope points from Mach (M) 0.2 to 0.7, height (h) 0m to 9750m. The model is a look-up table for force and moments in the body frame at various CG locations and consists of the dependencies as shown in Table 1.

Table 1 Force and moment aerodynamic coefficients, r and v denotes RANS and VLM simulations respectively, and i denotes inner elevon and o outer elevon. Adapted from [19]

at: $M/h/x_{cg}$	α	β	$\hat{p}$	$\hat{q}$	$\hat{r}$	$\delta_{e_{i/o}}$	$\delta_{a_{i/o}}$	δ_r
C_X	r					r	r	r
C_Y		r			v		r	r
C_Y	r			v		r		
C_l		r	v		v		r	r
C_m	r			v		r		
C_n		r	v		v		r	r

The aerodynamic coefficients for the control surfaces are modelled as ganged control surfaces with elevator deflection (δ_e), aileron deflection (δ_a) for the inner and outboard elevons. These respective aerodynamic coefficients will be split separately for each control surface with the assumption that the deflection of a single elevon will account for 50 % of the performance brought by the deflection of either both, as elevator, or asymmetrically, as aileron. The rudders on the winglet will be kept as they are. The tabulated aerodynamic data is also interpolated linearly.

The aircraft parameters concerning mass and CG are established in [18], assuming a family optimised Flying V, FV-1000 aircraft, which defines a Maximum Take-off Weight (MTOW) of 266 tonnes and a Maximum Landing Weight (MLW) 76% of its MTOW. The most forward (longitudinal) position of CG with MLW is at approximately 28.5m, distanced from the nose, and 29.1m at MTOW, the most aft position is 30.1m. The moment of inertia is determined through a lumped mass method as established in [2] and is a source of uncertainty as it has not been updated with the new geometry and aerodynamic model. The mean aerodynamic chord ($\bar{c}$) is 18m, the surface (S) is 898 m^2 and the span (b) is 65 m.

C. Actuators

The control surface actuators are modelled as an 2nd order system:

$$H_{act} = \frac{\omega_0^2}{s^2 + 2\zeta\omega_0 s + \omega_0^2} \tag{1}$$

The engine is modelled as a first order system with a maximum thrust of 379 kN [5]:

$$H_{eng}(s) = \frac{1}{0.2s + 1} \tag{2}$$

The elevon and rudder actuator dynamics and properties shown in Table 2 were based upon the actuator parameters defined for a large transport aircraft Boeing 747 [22, 23], which is changed from the actuator dynamics that were derived from more agile aircraft [5]:

Table 2 Control Surface actuator limits and actuator parameters

	Inboard and outboard elevons ($\delta_{CS1}^{L/R}$ & $\delta_{CS2}^{L/R}$) min,max	Rudder ($\delta_{CS3}^{L/R}$) min, max
Position limits ($\dot{u}$) [deg]	-25,25	-30,30
Rate limits (u) [deg/s]	-40,40	-45,45
Natural frequency (ω_0) [rad/s]	35	35
Damping coefficient (ζ) [-]	0.8	0.8

D. Rigid Body Dynamics

The rigid body dynamics and aerodynamic coefficients are defined in the body-fixed reference frame ($\mathcal{F}_\mathcal{B}$) as shown in Figure 2.

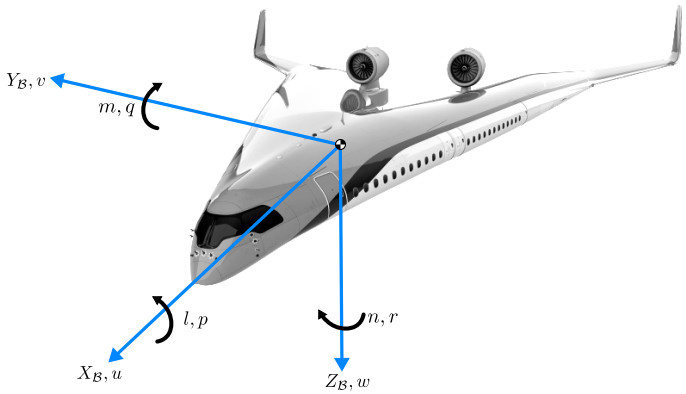

Fig. 2 Aircraft body axes and conventions. Adapted from [2]

The following assumptions are made to describe the equations of motion of the aircraft [3]; 1) The aircraft is a rigid body and has constant mass, 2) The Earth is flat and non-rotating and inertial reference frame, 3) There is zero wind and a perfect atmosphere, 4) The aircraft has a plane of symmetry such that $I_{xy} = I_{yz} = 0$ and thrust lies in the symmetry plane, 5) The gravitational acceleration is constant.

The forces acting on the aircraft consist of gravity, propulsion forces and aerodynamic forces. It is assumed that the distributed forces can be replaced with point forces that generate moments around the center of gravity. With the flat and non-rotating Earth assumption, the vehicle-carried normal Earth reference frame is similar to an inertial reference frame. The equation of motion for the simulation model describes a 6-Degree of Freedom (DOF) dynamic system and is formed by the translational dynamics, rotational dynamics, and the kinematics. The complete set of equations of motion for 6-DOF simulation is defined as:

$$
\begin{aligned}
\dot{x_E} &= (u\cos(\theta) + (v\sin(\phi) + w\cos(\phi))\sin(\theta))\cos(\psi) - (v\cos(\phi) - w\sin(\phi))\sin(\psi) \\
\dot{y_E} &= (u\cos(\theta) + (v\sin(\phi) + w\cos(\phi))\sin(\theta))\sin(\psi) + (v\cos(\phi) - w\sin(\phi))\cos(\psi) \\
\dot{z_E} &= -u\sin(\theta) + (v\sin(\phi) + w\cos(\phi))\cos(\theta) \\
\dot{u} &= vr - wq - g\sin(\theta) + \frac{F_X}{m} \\
\dot{v} &= wp - ur + g\sin(\phi)\cos(\theta) + \frac{F_Y}{m} \\
\dot{w} &= uq - vp + g\cos(\phi)\cos(\theta) + \frac{F_Z}{m} \\
\dot{p} &= \frac{I_{zz}}{I^*}M_X + \frac{I_{xz}}{I^*}M_Z + \frac{(I_{xx} - I_{yy} + I_{zz})I_{xz}}{I^*}pq + \frac{((I_{yy} - I_{zz})I_{zz} - I_{xz}^2)}{I^*}qr \\
\dot{q} &= \frac{M_Y}{I_{yy}} + \frac{(r^2 - p^2)I_{xz}}{I_{yy}} + \frac{(I_{zz} - I_{xx})}{I_{yy}}pr \\
\dot{r} &= \frac{I_{xz}}{I^*}M_X + \frac{I_{xx}}{I^*}M_Z + \frac{((I_{xx} - I_{yy})I_{xx} + I_{xz}^2)}{I^*}pq + \frac{(-I_{xx} + I_{yy} - I_{zz})I_{xz}}{I^*}qr \\
\dot{\phi} &= p + \sin(\phi)\tan(\theta)q + \cos(\phi)\tan(\theta)r \\
\dot{\theta} &= \cos(\phi)q - \sin(\phi)r \\
\dot{\psi} &= \frac{\sin(\phi)}{\cos(\theta)}q + \frac{\cos(\phi)}{\cos(\theta)}r
\end{aligned}
\tag{3}
$$

With I^* defined as followed:

$$
I^* = I_{xx} * I_{yy} - I_{xx}^2 \tag{4}
$$

The forces and moments are defined as followed:

$$
\begin{aligned}
F_X &= F^B_{X_{\text{aero}}} + F^B_{grav_X} + T_1 + T_2 \\
F_Y &= F^B_{Y_{\text{aero}}} + F^B_{grav_Y} \\
F_Z &= F^B_{Z_{\text{aero}}} + F^B_{grav_Z} \\
M_X &= M^B_{X_{\text{aero}}} \\
M_Y &= M^B_{Y_{\text{aero}}} - (T_1 + T_2)T_{dz} \\
M_Z &= M^B_{Z_{\text{aero}}} + (T_1 - T_2)T_{dy}
\end{aligned}
\tag{5}
$$

With T_1, T_2 the thrust force produced by the left and right engine and T_{dy}, T_{dz} are the respective moment arm lengths. The CG and reference position at which the aerodynamic forces act are described with x_{cg} and x_{ref} respectively. The body accelerations are calculated as:

$$
A_x = \frac{C_X}{m} - g\sin(\theta) \tag{6}
$$

$$
A_y = \frac{C_Y}{m} + g\sin(\phi)\cos(\theta) \tag{7}
$$

$$
A_z = \frac{C_Z}{m} + g\cos(\theta)\cos(\phi) \tag{8}
$$

With the 6-DOF simulation model an output state is also computed of 18 states are measured by the sensors.

E. Sensor Model

The sensors used in the Flying V simulation model are based upon the description provided in [5, 17], which based its sensor parameters on the specifications used in [24]. However, the baseline sensor parameter specifications would not obtain level 1 handling qualities for the Flying V, some adjustments were made to obtain that, and it is assumed that such sensors characteristics are obtainable. The sensor characteristics used for this research are shown in Table 3 .

Table 3 Sensor parameters, based on [24]

State	Noise (σ^2)	Bias	Delay [ms]	Sampling rate [Hz]	Filter time constant [s]
p, q, r [rad/s]	1.5×10^{-9}	3.0×10^{-5}	50	100	0.04
ϕ, θ, ψ [rad]	1.0×10^{-9}	4.0×10^{-3}	50	50	0.05
f_x, f_y, f_z [rad]	1.5×10^{-5}	2.5×10^{-3}	100	50	0.05
α, β [rad]	7.5×10^{-8}	3.0×10^{-3}	100	100	0.05
h [m]	4.5×10^{-3}	8.0×10^{-3}	150	20	0.05
V [m/s]	8.5×10^{-4}	2.5	150	20	0.05
δ_{CSi} [rad]	1.5×10^{-9}	2.5×10^{-5}	-	100	-

Additionally, noise and bias are also added to the control surface output, and these are assumed to be originated from the actuator sensors.

The model for the sensor dynamics and filtering is described in [5], where the sensors sample the state and are then filtered with a first order (discrete) filter, with their respective filter time constant. As the sensors do not provide direct measurements of the rotational accelerations $(\dot{p}, \dot{q}, \dot{r})$, to obtain these measurements a second order filter is applied on the gyroscope sensor, which measures the rotation rates (p, q, r) and are then computed with first order Euler differentiation. The filtering parameters for the second order filter are set to $\omega = 25$ and $\zeta = 0.75$.

III. Flight Control System Design

This section describes the baseline control architecture of the Flying V, which consist of inner loop rate control with INDI, outer loop controllers and at last tuning of the gains in the controller. The control architecture is derived from the implementation described in [5, 17], but Flight Envelope Protection (FEP) isn't implemented for this research. A complete overview of the controller is shown in Figure 3.

A. Outer Loop Control

This section will elaborate on the outer loop controllers and and is derived from the control structure as outlined in [5], where the outer loop control structure has several components, namely the:

1) C^* controller block with pitch reference model for longitudinal channel control, which has been adjusted in this research to not enable compensation near the pitch and roll attitude limits continuously, but only when it nears these limits.
2) A roll reference model for the roll channel control
3) Sideslip compensator for the yaw channel control
4) Linear Controller that computes a virtual control signal based on the references from the three aforementioned control blocks.
5) Speed controller to maintain the aircraft at the commanded trim speed
6) Pseudo-Control Hedging to prevent actuator wind-up by high (incremental) control commands

B. Incremental Nonlinear Dynamic Inversion (INDI) Rate Control

INDI is a nonlinear control law closely related to its model-based precursor, Nonlinear Dynamic Inversion (NDI), which aims to linearize a nonlinear system through the cancellation of nonlinear system dynamics with state feedback [25] and define a control law design where the inner loop behaves like an integrator, which can then be controlled by an outer loop linear controller, such as Proportional-Integral-Derivative (PID). One drawback of NDI is that it requires complete system knowledge and to overcome this drawback INDI uses sensor estimates for its control law design and reducing knowledge required of the system dynamics by using the control effectiveness (CE) model, thus requiring less model knowledge [26, 27]. This approach is derived derived for a nonlinear system through Taylor series expansion, at a current state and time point (x_0, u_0)

$$\mathbf{x} = \mathbf{f}(\mathbf{x}, \mathbf{u}) \tag{9}$$

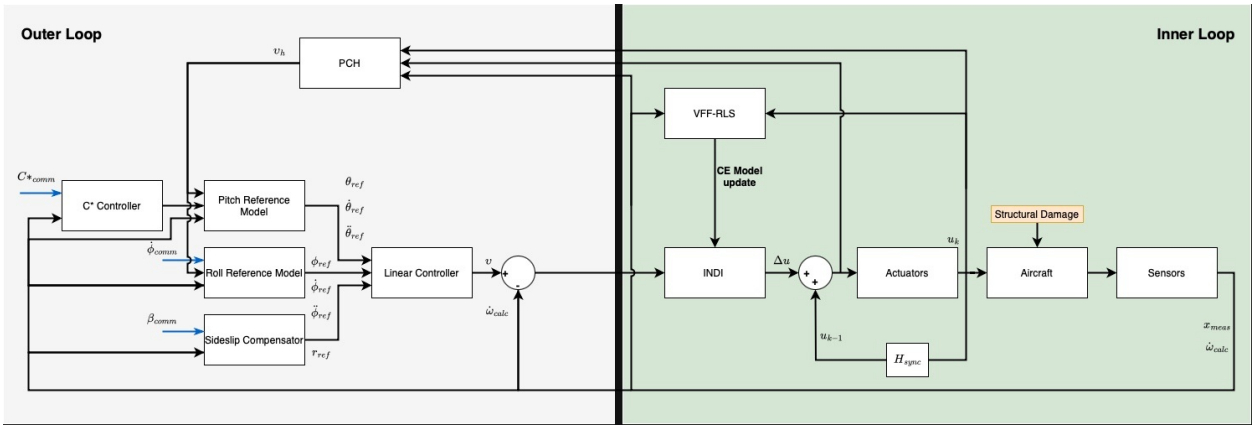

Fig. 3 Flight control system architecture. Modified from [17]

$$\dot{x} \approx f(x_0, u_0) + \frac{\partial f(x,u)}{\partial x}|_{x=x_0,u=u_0}(x - x_0) + \frac{\partial f(x,u)}{\partial u}|_{x=x_0,u=u_0}(u - u_0) \tag{10a}$$

$$\approx \dot{x}_0 + F((x_0, u_0))(x - x_0) + G(x_0, u_0)(u - u_0) \tag{10b}$$

$$\approx \dot{x}_0 + F((x_0, u_0))\Delta x + G(x_0, u_0)\Delta u \tag{10c}$$

Applying the time-scale separation principle, the linearisation is simplified and thereafter an incremental control law can be derived:

$$\dot{x} \approx \dot{x}_0 + G(x_0, u_0)\Delta u \tag{11}$$

$$\Delta u = G^{-1}(x_0, u_0)(v - \dot{x}_0) \tag{12}$$

Whereby $G(x_0, u_0)$ is the control effectiveness matrix, ν is the desired virtual reference from the outer loop controller and x_0 is the currently measured state estimate from the sensors and Δu is the incremental control command. By adding the previously measured control surface deflection, the control command to the actuators can be determined:

$$u = u_0 + \Delta u \tag{13}$$

For the application of INDI the following assumptions are implicitly made [26, 28, 29]:

1) Complete and accurate knowledge of states is available
2) Sensors to measure the acceleration **x** with sufficiently high sampling rate need to exist and be available
3) Sensor to measure the current control input (actuator) need to be available or estimated on the basis of a high-fidelity model of the actuator dynamics
4) Time-scale seperation where it is assumed that the state derivatives evolve faster than the state upon fast control action, which directly influences the dynamics of the rigid body
5) Fast control action is assumed, where the dynamics of the actuator (and control surface) evolve much faster than the states
6) Control effectiveness matrix is invertible

The derivation of INDI for rate control is obtained by first order Taylor Series approximation at the linearization state and input of the angular dynamics (ω) with the assumption of time-scale separation and sufficiently high sampling time:

$$\dot{\omega} = \mathbf{J^{-1}M} - \mathbf{J^{-1}\Omega J}\omega \tag{14}$$

$$\dot{\omega} \approx \dot{\omega}_0 + F\Delta\mathbf{x} + G\Delta\mathbf{u} \tag{15}$$

$$\dot{\omega} \approx \dot{\omega}_0 + G\Delta\mathbf{u} \tag{16}$$

The control effectiveness matrix G is in Equation 18, with the control effectiveness coefficients ($C_{*_{\delta_{CS}^{L/R}}}$), which is the aerodynamics moment coefficients with respect to each control surface and rolling moment, are determined through the

linearization of the dynamics.

$$\Delta \mathbf{u} = G^{-1}(\omega_{des} - \omega_0) \tag{17}$$

$$G = \frac{\bar{q} * S}{\mathbf{I}} \begin{bmatrix} b & 0 & 0 \\ 0 & c & 0 \\ 0 & 0 & b \end{bmatrix} \begin{bmatrix} C_{l_{\delta^L_{CS1}}} & C_{l_{\delta^R_{CS1}}} & C_{l_{\delta^L_{CS2}}} & C_{l_{\delta^R_{CS2}}} & C_{l_{\delta_{CS3}}} \\ C_{m_{\delta^L_{CS1}}} & C_{m_{\delta^R_{CS1}}} & C_{m_{\delta^L_{CS2}}} & C_{m_{\delta^R_{CS2}}} & C_{m_{\delta_{CS3}}} \\ C_{n_{\delta^L_{CS1}}} & C_{n_{\delta^R_{CS1}}} & C_{n_{\delta^L_{CS2}}} & C_{n_{\delta^R_{CS2}}} & C_{n_{\delta_{CS3}}} \end{bmatrix} \tag{18}$$

$$C_{*_{\delta^{L/R}_{CS}}} = \frac{\partial C_m}{\partial \delta^{L/R}_{CSi}} \tag{19}$$

The control effectiveness is not squared and can not be inverted, for which there are more control surfaces available for generating a specific moment on the aircraft. A control allocation algorithm is used that makes the most effective choice on which control surface has been used, computed with the Moore-Penrose pseudoinverse [30] as:

$$\mathbf{P} = \mathbf{G}^T(\mathbf{G}\mathbf{G}^T)^{-1} \tag{20}$$

The incremental command is added with the previously known control surface deflection to form the commanded input to the actuators.

$$\mathbf{u} = \mathbf{u}_0 + \underbrace{\mathbf{P}(\mathbf{v} - \mathbf{x_0})}_{\Delta u} \tag{21}$$

One crucial aspect of applying INDI is its synchronization of the control deflections with the measurements of the sensors [26, 31, 32], as the control surface and sensor dynamics are not directly available, some latency occurs and if not accounted for, it can result in oscillatory response. To compensate for this, the sampling and filtering of the measurement from the actuators is performed with the same filtering as the body rate sensor, which is an 2^{nd} older filter, and a pure time delay to compensate for any difference between both sensors [26]. In this research, an additional time delay of $5ms$ is added.

C. Adaptive INDI Control Law

This section concerns the adaptation of control effectiveness through the correction with a scaling parameter, which is a lumped term that corrects for any mismatch between the onboard and real control effectiveness and has been employed in previous studies [16] and research presented by Swain & Manickavasagar in [13] used a FTC with Fault Detection and Identification for optimal control allocation by identifying a failure of a control surface through it's desired control demand and achieved control demand with a Kalman filter.

For this research's implementation each term in the control effectiveness matrix G is thus scaled as followed:

$$\tilde{G}_{ij} = \theta_{ij} G_{ij} \tag{22}$$

The prediction model is determined from the INDI control law, where the current on board model is used for the estimation and the prediction error is the residual of the incremental change of angular acceleration of the aircraft and the incremental deflection to achieve the desired change. The derivation of the residual is obtained through the following steps. First, the linearized equation of the angular dynamics with the assumption of time-scale separation is formulated.

$$\dot{\omega}_k \approx \dot{\omega}_{k-1} + \tilde{G}_{k-1}\Delta(u_k - u_{k-1}) \tag{23}$$

The previous angular acceleration as measured by the sensors $\dot{\omega}_{k-1}$ is brought to the left hand side, and an incremental change in rate acceleration is obtained.

$$\Delta\dot{\omega} = \dot{\omega}_k - \dot{\omega}_{k-1} = \tilde{G}_{k-1}\Delta\mathbf{u} \tag{24}$$

This incremental change on the left hand side should be proportional to the incremental change on the right hand side and thus the following residual is derived:

$$\epsilon = \Delta\dot{\omega}_{ij} - (\tilde{G}_{ij})_{k-1}\Delta\mathbf{u}_j \tag{25}$$

1. Recursive Least Squares

Recursive least squares algorithm has been used in various adaptive control studies for online identification and adaptation of control parameters. The algorithm can be formally described with three steps [33, 34]:

$$K_k = P_{k-1}X_{k-1}(\lambda_k + X_{k-1}^T P_k X_{k-1})^{-1}$$
$$\hat{\theta}_k = \hat{\theta}_{k-1} + K_k \epsilon_k$$
$$P_k = \frac{1}{\lambda}(P_k - K_k X_{k-1} P_k)$$

Where K is the gain, that corrects and updates the current parameter estimation.One main disadvantage of recursive identification is that when there is no excitation or "information richness" in the estimator, old information is continuously forgotten and this results in an exponentially growing covariance matrix, which could destabilise the system and parameter estimation. One solution is to employ a variable forgetting factor, which is tuned based on the information content (Σ_0) of the filter and continuously adjust the forgetting factor to keep the information content constant. This has the following formulation for the forgetting factor [34, 35]:

$$\lambda = 1 - \frac{[1 - \phi_k K_k]\epsilon^2}{\Sigma_0} \tag{26}$$

Setting the information constant can be done by expressing it with relation to the expected measurement noise with a nominal memory length (N_0) expressed as:

$$\Sigma_0 = \sigma_0^2 N_0 \tag{27}$$

Algorithm 1 Recursive least squares: parameter estimation

input: $\omega_{\mathbf{k}}, \omega_{\mathbf{k-1}}, \mathbf{U_k}, \mathbf{U_{k-1}}, \hat{\theta}_{\mathbf{k}}, \mathbf{P}_k, \lambda_k, C_{*_{\delta_{CS}^{L/R}}}$
initialization: $\hat{\theta}_{\mathbf{0}}, \mathbf{P}_0, \lambda_0, \mathbf{J}, \bar{q}, S, c, b$
while $k \leq N$ **do**
  $z_{k+1} = \dot{\omega}_k - \dot{\omega}_{k-1}$
  $\Delta\mathbf{U}_k = \mathbf{U}_k - \mathbf{U}_{k-1}$
  $\phi_{k+1} = \frac{\bar{q}*S}{\mathbf{I}} diag\left(\begin{bmatrix} b & c & b \end{bmatrix}\right) C_{*_{\delta_{CS}^{L/R}}} \Delta\mathbf{U}_k$
  $\epsilon_k = z_{k+1} - \phi_{k+1}^T \hat{\theta}_k$
  $\Delta\theta_{k+1} = \mathbf{0}^{3x5}$
  for $i \leq 3$ **do**
    $K_{k+1} = \frac{P_k(i)\phi_{k+1}(i)}{(\lambda_k(i) + \phi_{k+1}^T P_k(i)\phi_{k+1}(i))}$
    $\Delta\theta_{k+1}(i) = K_{k+1}\epsilon_k(i)$
    $\lambda_k(i) = \max(\lambda_{\min}, \max(\lambda_{max}, 1 - (1 - \phi_{k+1}^T K_{k+1})\frac{e_k(i)^2}{\Sigma_0})$
    $P_{k+1} = \lambda^{-1}\left(P_k - K_{k+1}\phi_{k+1}^T P_k\right)$
  end for
  for $j \leq 5$ **do**
    $\Delta\bar{\theta}_{k+1}(j) = \frac{\sum_{i=0}^{3}\Delta\theta_{k+1}(i,j)}{3}$
    for $i \leq 3$ **do**
      if $|\Delta\theta_{k+1}(i,j) - \Delta\bar{\theta}_{k+1}(j)| >$ 1e-6 **then**
        $\Delta\theta_{k+1}(i,j) = \Delta\bar{\theta}_{k+1}(j)$
      end if
      $\hat{\theta}_{k+1}(j) = \hat{\theta}_k(j) + \Delta\theta_{k+1}(j)$
    end for
  end for
end while

By setting the value of, Σ_0 the filter adapts new information more quickly or slower, as the covariance matrix increases and becomes more sensitive. Thus, the speed of the adaptation is determined by how small of a value Σ_0 is set

to, and a larger value increases the robustness of the parameter estimate. The variable forgetting factor also plays a crucial role for estimating sudden changes in CE, as new information becomes essential for the adaptation.
The RLS algorithm is applied in the adaptive control law, where it computes and adapts the correction parameter per row, which corresponds to all control surfaces per axis of the rate acceleration. One practical adjustment has been made with the correction parameter, which is that the respective update corresponding to each control surfaces is ensured to be proportionally similar. This is done by first storing the respective updates for each axis, and then applying that update if they conform to the same relative threshold, otherwise the mean correction for that control surface is applied and thus the magnitude of the correction is constrained for each row (axis moment) and column (control surface effectiveness). This also accounts for the noise that's present in the measurement by the sensors.

For the Flying V FCS, the virtual control hedge is subtracted for the pitch and roll reference model, but not sideslip compensator with respect to the yaw rate.

D. Fault injection

The simulation model has been updated to insert structural faults into the aircraft model. These faults are done through scaling, where the original aerodynamic coefficients for the control surface forces and moments are modified to introduce structural damage as described in [17]. Thus, the original coefficient of the respective control surface is scaled as following:

$$\tilde{C}_{*_{\delta_{CS}^{L/R}}} = \mu \cdot C_{*_{\delta_{CS}^{L/R}}} \tag{28}$$

With $\mu \in (1, 0)$, where 1 means it has full control effectiveness and 0 means that the control effectiveness is lost.

E. Tuning

The tuning of the gains in the outer loop control blocks are done through a multi-objective optimisation, as performed by Stougie [5]. However, the tuning routine was performed through trial-and-error with random sampling of gains until various objectives were minimized and constraints were satisfied. This section elaborates first on the bare-airframe dynamics at the selected flight condition, thereafter a new tuning routine through a Multi-Objective Parameter Synthesis (MOPS) is elaborated and at last the tuning results are presented.

1. Bare-airframe dynamic modes

Before the aircraft is tuned, the aircraft is trimmed at their respective flight conditions and the decoupled into longitudinal and lateral dynamics analyse the dynamic modes of the aircraft. The eigenvalues are shown in Figure 4 & 5 respectively, where it can be shown that at each respective flight condition, the phugoid is near the right half pole plane nearing instability with exception to the Takeoff condition where it is unstable. The Lateral eigenvalues reveal that the Dutch roll is also nearing instability, and all flight conditions have unstable spirals. This reveals that the bare-airframe dynamics require stability augmentation systems to fly the aircraft trimmed at the flight conditions.

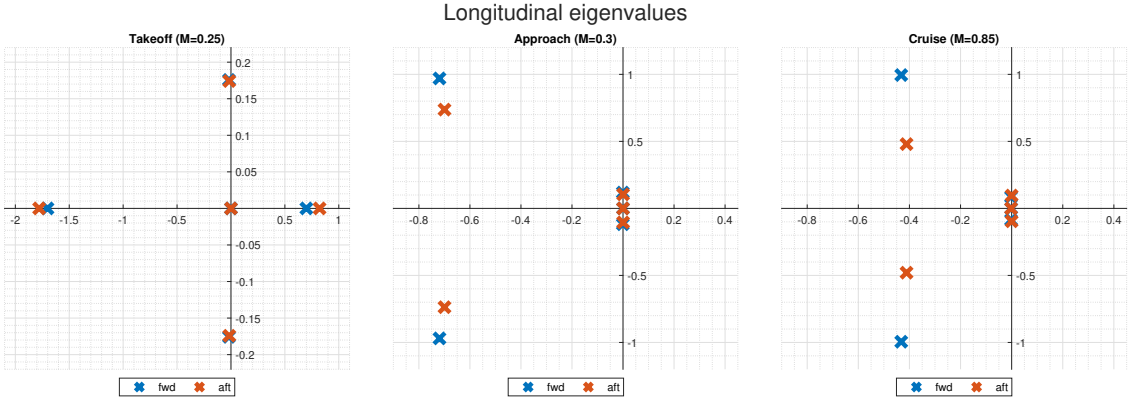

Fig. 4 Longtiudinal eigenvalues at forward and aft centre of gravity for three flight conditions

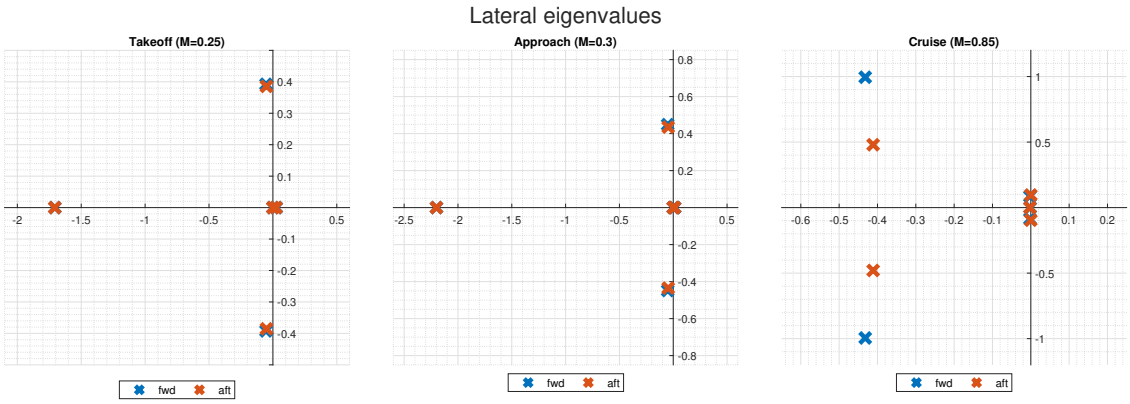

Fig. 5 Lateral eigenvalues at forward and aft centre of gravity for three flight conditions

This research will focus on the Approach flight condition, as it is a critical flight condition in aircraft operation.

2. Multi-Objective Parameter Synthesis tuning routine

The tuning of the gains in the outer loop control blocks are done through a multi-objective optimisation, extensively described by Stougie [36]. However, tuning was done through trial-and-error with random sampling of gains until various objectives were minimized and constraints were satisfied. This section elaborates the tuning routine with Multi-Objective Parameter Synthesis (MOPS) is elaborated and at last the tuning results are presented.

The optimisation method applied for the tuning is the *pattern search* optimisation in MATLAB [†], which is a direct search method that finds a set of points based on the current point at each iteration and approach an optimal point where the value of the objective function either decreases or remains the same for iteration. The optimisation is performed separately for the longitudinal and lateral design parameters, and the objective function is based upon the scoring for the following objectives [36]:

- The MIL-STD-179A flying and handling quality requirements [37–39]
- Stability margins, Gain and Phase, which is computed at the broken loop location just before the INDI control block in Figure 3 [40]
- Low Order Equivalent System (LOES) fit [37, 41]
- Attitude bandwidth for longitudinal control [42]
- Tracking performance with block inputs

For the tracking response, the following metrics are computed:

1) Root Mean Squared Error (RMSE), which quantifies the average error and penalises high deviations
2) $\delta_{CS_{activity}}$, which penalises high deflections, and thus high actuator rates
3) Risetime, Settlingtime, Overshoot all quantify the transient response to the tracking reference and obtained using the *stepinfo* function in MATLAB

$$RMSE = \sqrt{\sum_{i=0}^{N} \frac{(y_{r_i} - y_i)^2}{N}} \qquad \delta_{CS_{activity}} = \frac{\int_0^{T_{sim}} (\dot{\delta})^2}{T_{sim}} \tag{29}$$

The objectives are formulated to a composite scoring objective function where the constraints are either minimized or normalized, and then weighed proportionally to have a similar magnitude in the objective function. This weighing is defined according to trial and error. The level of flying qualities, are penalized proportionally depending on the thresholds of its flying quality with a weighed from 1 to 1000. Table 4 and 5 summarise all the objectives.

$$HQ_{i_{normalized}} = W_{FQ_i} * \left(\frac{HQ_{obtained} - HQ_{boundary}}{HQ_{desired}} \right)^2 \tag{30}$$

$$HQ_{i_{minimized}} = W_{FQ_i} * \left(HQ_{boundary} - HQ_{obtained} \right)^2 \tag{31}$$

$$\tag{32}$$

[†]https://nl.mathworks.com/help/gads/how-pattern-search-polling-works.html

The final objective is defined as a composite scoring between the handling quality and tracking performance as:

$$Score = HQScore + TQScore \tag{33}$$

The optimisation was performed until a minimum was found, however, due to the high computational time of the tuning the maximum evaluations for the optimisation was set at 320 function evaluations.

Table 4 Longitudinal tuning objectives [5, 40]

Longitudinal tuning objectives					
		Min		Max	
Description	**Type**	**B**	**C**	**B**	**C**
Response to C* block command of $\Delta C^* = 0.25$, T_{sim} = 35					
RMSE	Min		-		-
$CS_{activity}$	Min		-		-
x_{max}	Min		-		-
RS [s]	Min		-		-
ST [s]	Min		-		-
OS [%]	Min		10%		-
Linear Analysis					
GM v_q [dB]	Constr.		6		-
PM v_q [°]	Constr.		45		-
ω_{sp} [rad/s]	Constr.	-	0.87		-
ζ_{sp} [-]	Constr.		0.30 / 0.50		2.0 / 1.3
CAP [$g^{-1}s^{-2}$]	Constr.		0.085 / 0.16		3.6
$score_{LOES}$ [-]	Constr.		-		15

Table 5 Lateral tuning objectives [40]

Lateral tuning objectives					
		Min		Max	
Description	**Type**	**B**	**C**	**B**	**C**
Response to $\dot{\phi}$ block command of ±3°, $T_{sim} = 45s$					
RMSE	Min		-		-
$\Delta\beta$	Min		-		-
$CS_{activity}$	Min		-		-
x_{max}	Min		-		-
RS [s]	Min		-		-
ST [s]	Min		-		-
OS [%]	Min		10%		-
Linear Analysis					
GM v_p [dB]	Constr.		6		-
PM v_p [°]	Constr.		45		-
GM v_r [dB]	Constr.		6		-
PM v_r [°]	Constr.		45		-
$1/T_s$ [s^{-1}]	Constr.		-0.035 / -0.058		-
T_r [s]	Constr.		-		1.4 / 1.0
ω_{dr} [rad/s]	Constr.		0.5		-
ζ_{dr} [–]	Constr.		0.08		-
$\omega_{dr}\zeta_{dr}$ [rad/s]	Constr.		0.15 / 0.10		-
$score_{LOES}$ [–]	Constr.		-		15

The system is trimmed, and tuned for the approach condition (M=0.3, H=1km) with forward center of gravity (28.5) at MLW, and the results are presented in Table 6 and Table 7 for the longitudinal and lateral respectively, where the yellow coloured cells indicate criteria, which hasn't been fulfilled. The tracking of the references used in the tuning is shown in Figure 6 & 7.

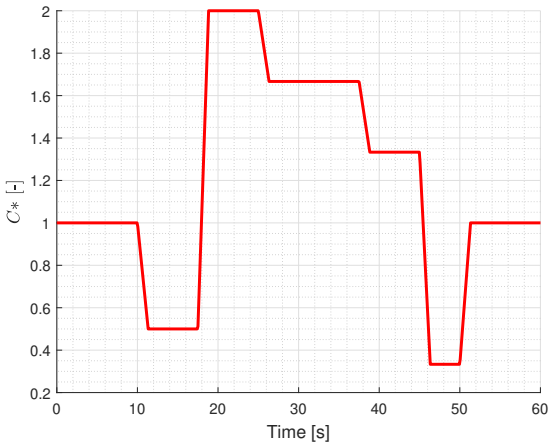

Fig. 6 Longitudinal C* tracking signal

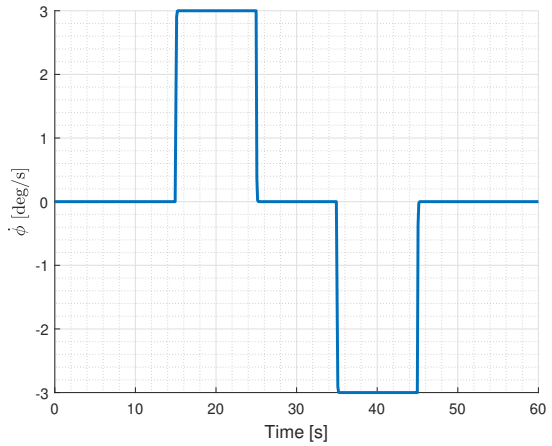

Fig. 7 Lateral $\dot{\phi}$ tracking signal

Table 6 Longitudinal tuning results

Description	Value
Linear analysis	
GM v_q [dB]	4.66
PM v_q [°]	51.18
ω_{sp} [rad/s]	1.39
ζ_{sp} [–]	0.65
CAP [$g^{-1}s^{-2}$]	0.32
$score_{LOES}$ [–]	2.53
Tracking quality	
OS	6.88 %
Risetime	0.48 s
Settlingtime	3.04 s
δ_{energy}	4.54 $\circ/s^2$

Table 7 Lateral tuning results

Description	Value
Linear Analysis	
GM v_p [dB]	5.93
PM v_p [°]	45.11
GM v_r [dB]	-7.62*
PM v_r [°]	42.35
$1/T_s$ [s^{-1}]	stable
T_r [s]	0.0793
ω_{dr} [rad/s]	7.26
ζ_{dr} [-]	2.48
$\omega_{dr}\zeta_{dr}$ [rad/s]	18.04
$score_{LOES}$ [–]	6.20
Tracking quality	
OS	12.832%
Risetime	1.19 s
Settlingtime	4.34 s
δ_{energy}	22.78 $\circ/s^2$

*smallest negative margin

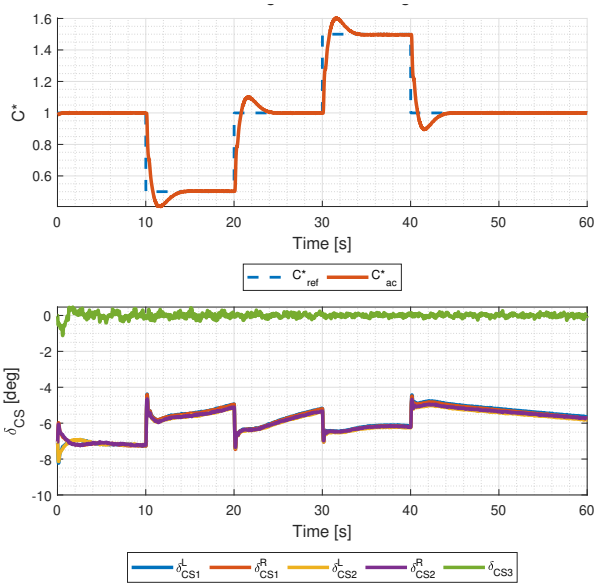

Fig. 8 Longitudinal tuned tracking response

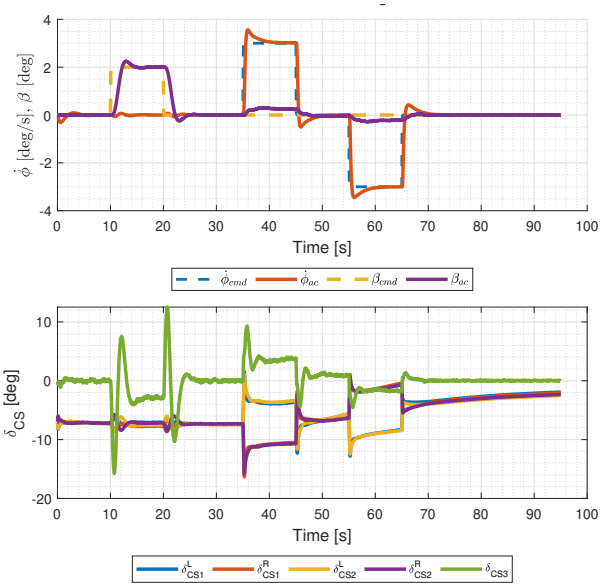

Fig. 9 Lateral tuned tracking response

IV. Results

In this section the numerical results are obtained for the approach flight condition at Mach = 0.3, Height = 1000m with a forward center of gravity. For the analysis the following tracking signals are used, for the C* command and roll rate command respectively, with a zero sideslip command. These signals are combined for longitudinal and lateral input tracking, shown in Figure 8 & 9.

An asymmetric structural fault is introduced as the inboard elevon has higher control authority for the longitudinal

channel and the outboard elevon has higher control authority for the roll channel, thus in a fault cause the healthy control surfaces are mainly responsible for reference tracking. The analysis was conducted in an incremental manner, where first a fault was introduced on the inboard elevon, left-hand side with increments of [1, 0.75, 0.5, 0.25, 0], where a value of 1 describes the control surface at full health and 0 means it has lost all of its effectiveness. Afterwards, a fault is introduced on the outboard elevon on the right-hand side, with the same increments. After the fault has been injected, a doublet signal is commanded for each elevon to excite the aircraft dynamics and create excitation for the parameter estimation.

The most severe case is presented when the respective faulty surfaces completely lose their effectiveness, which leads to degraded tracking, however with adaptation the tracking improves as shown by the results in Figure 10.

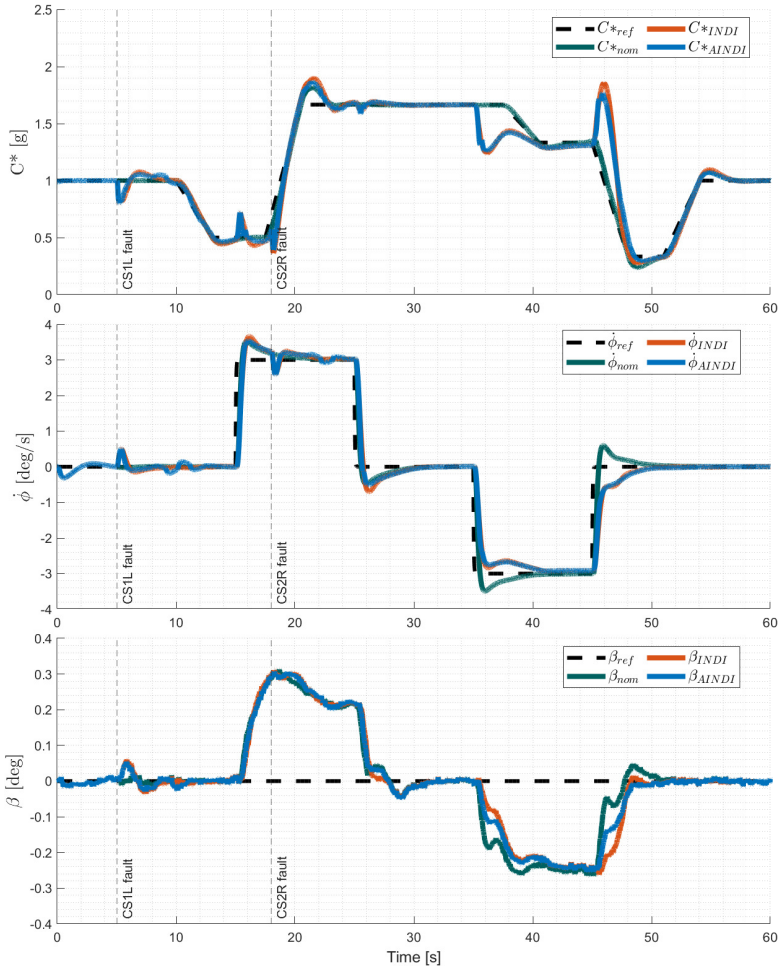

Fig. 10 C*, $\dot{\phi}$ and β control tracking comparison

The RMS for each tracking reference is shown in the Table 8, where it can be observed that the adaptive INDI is able to retain a lower RMSE compared to INDI in the presence of fault.

Table 8 RMSE of tracking responses

	Nominal		**Fault case**	
Tracking input	INDI	AINDI	INDI	AINDI
$\dot{\phi}$ [deg/s]	0.3233	0.3222	0.3877 (+20%)	0.3776 (+17%)
C*	0.0322	0.0313	0.1249 (+287%)	0.1129 (+260%)
β [deg]	0.1093	0.1095	0.1084 (−3%)	0.1072 (−2%)

In Figure 11 & 12 it can be observed that without adaptation, as the fault is introduced the control surfaces deflect

proportionally to the loss in effectiveness. However, with adaptation, the control surfaces are excited, and their deflection is changed as shown in Figure 13 & 14 due to the adaptation of its control effectiveness. This is further examined by the adaptation of the control effectiveness relative to the true control effectiveness of the aircraft dynamics shown in Figure 15, where the respective entries of the control effectiveness matrix correspond to the row and column respectively, here $\hat{G}(1,2)$ corresponds to the right hand inboard elevon control effectiveness estimation. It can be observed that the affected control surfaces on the left and right-hand side adjust proportionally, however as there is no excitation in the yaw channel, its control effectiveness does not show a significant difference as the change in sideslip angle was not perturbed significantly. The underestimation of the non-faulty CE terms lead to increased control effort by the respective control surfaces and thus account for the loss of effectiveness of the other control surfaces.

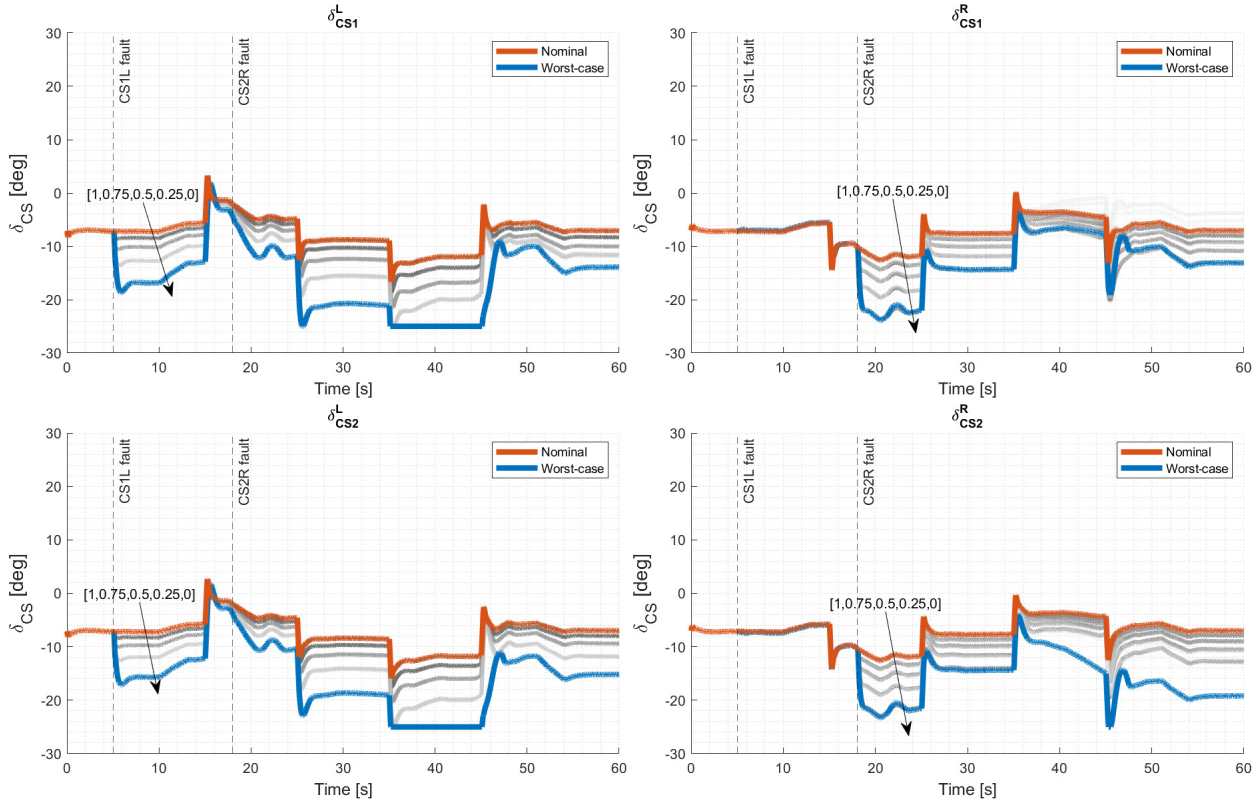

Fig. 11 INDI: Control surface deflection with fault on inboard elevon δ^L_{CS1} and outboard elevon δ^R_{CS2} in increments

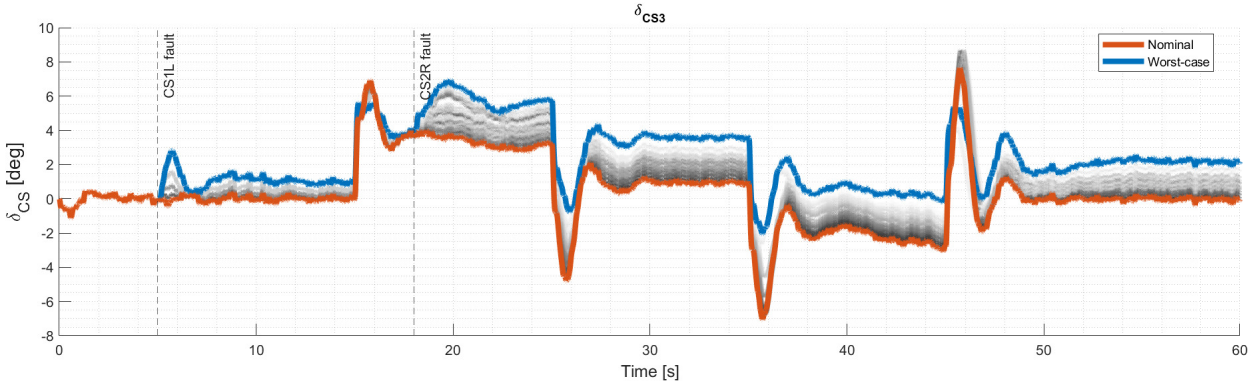

Fig. 12 INDI: Control surface deflection with fault on rudders δ_{CS3} in increments

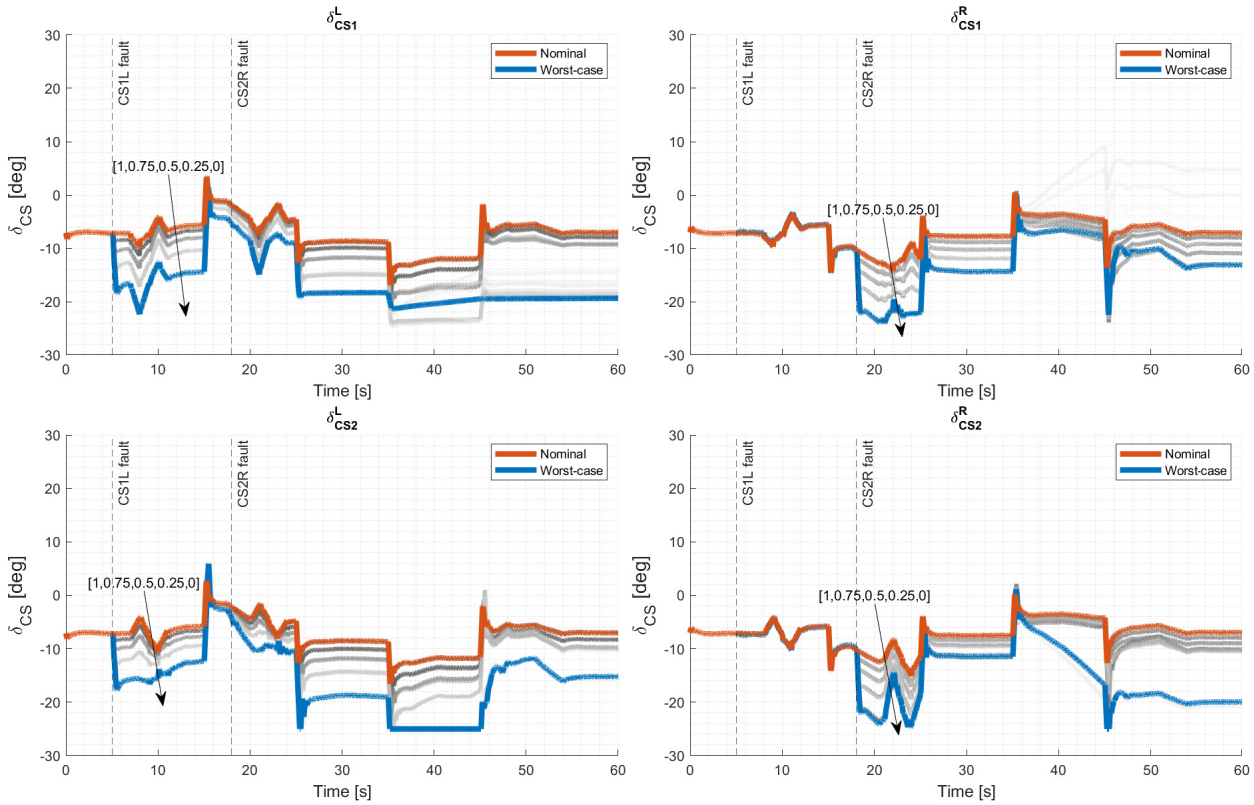

Fig. 13 AINDI: Control surface deflection with fault on inboard elevon δ^{L}_{CS1} and outboard elevon δ^{R}_{CS2} in increments

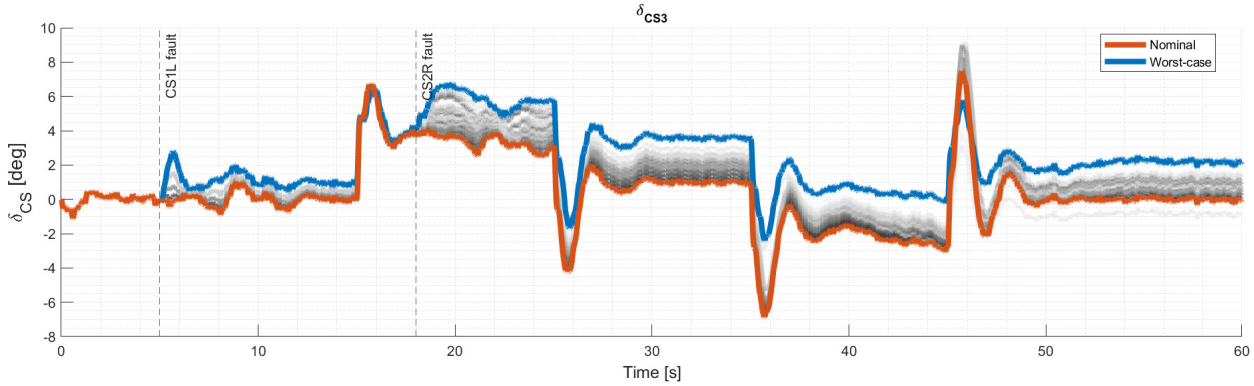

Fig. 14 AINDI: Control surface deflection with fault on rudders δ_{CS3} in increments

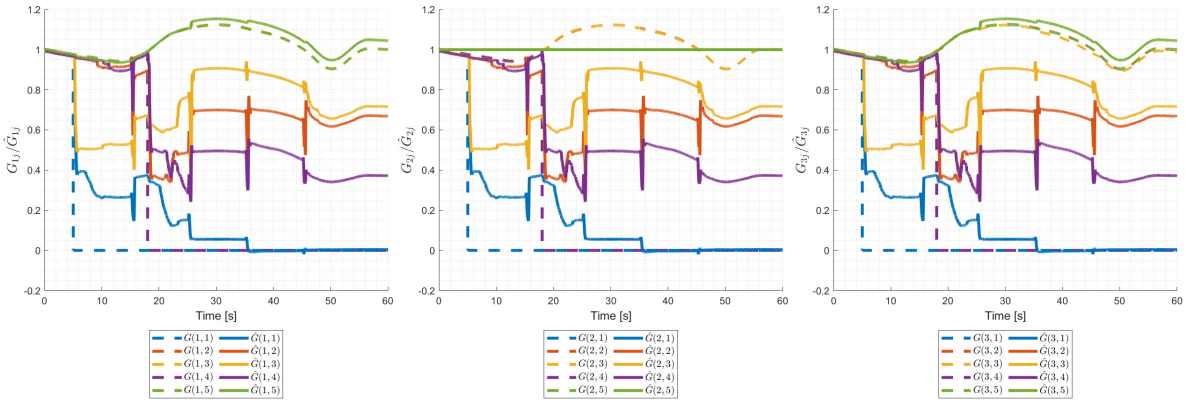

Fig. 15 Relative Control effectiveness estimation

V. Conclusion

In this research adaptive Incremental Nonlinear Dynamic Inversion (INDI) has been applied in the inner loop for rate control to adapt the onboard Control Effectiveness (CE) and account for model mismatches and faults. INDI has been known to be robust against model uncertainties, however in cases like limited control authority and faults, the concern of performance degradation could impede on safe and operable flight. These results establish how adaptation of the onboard CE used with INDI control law improves performance in the presence of faults such as loss of effectiveness. The CE model is adapted through a scaling parameter that corrects the currently estimated onboard model. This simple structure allows a generalisable implementation without prior-knowledge of the underlying model parameter structure, however, as non-linearities are not captured with this lumped correction term, different parameter models may be required. Further analysis of more challenging fault scenarios to observe how adaptation can maintain satisfactory performance tracking, where sensor faults and actuator faults can be performed. In addition, the excitation is triggered after the fault is injected, which is not known beforehand, with a doublet excitation signal. It is challenging to perform in a closed loop system without influencing the dynamics and potentially even destabilising the aircraft, thus the identification of an adaptation trigger and an optimal excitation could further improve accurate identification. Lastly, noise, disturbances and time delays and even loss of sensors influence the adaptations and needs to be analysed in further analysis.

References

[1] van der Sman, E., Peerlings, B., Kos, J., Lieshout, R., and Boonekamp, T., *Destination 2050*, Report, Netherlands Aerospace Centre NLR, 2021. URL `https://www.destination2050.eu/wp-content/uploads/2021/03/Destination2050_Report.pdf`.

[2] Cappuyns, T., *Handling Qualities of a Flying V Configuration*, MSc. Thesis, Delft University of Technology, 2019. URL `https://resolver.tudelft.nl/uuid:69b56494-0731-487a-8e57-cec397452002`.

[3] Van Overeem, S., *Modelling, Control, and Handling Quality Analysis of the Flying-V*, MSc. Thesis, Delft University of Technology, 2022. URL `https://resolver.tudelft.nl/uuid:7fd04eec-41d4-4967-b246-89fdfac2446e`.

[4] van Overeem, S., Wang, X., and Van Kampen, E.-J., "Handling Quality Improvements for the Flying-V Aircraft using Incremental Nonlinear Dynamic Inversion," *AIAA SCITECH 2023 Forum*, American Institute of Aeronautics and Astronautics, Reston, Virginia, 2023. https://doi.org/10.2514/6.2023-0105.

[5] Stougie, J., Pollack, T., and Van Kampen, E.-J., "Incremental Nonlinear Dynamic Inversion control with Flight Envelope Protection for the Flying-V," *AIAA SCITECH 2024 Forum*, American Institute of Aeronautics and Astronautics, Reston, Virginia, 2024. https://doi.org/10.2514/6.2024-2565.

[6] Atmaca, D., Stroosma, O., and Van Kampen, E.-J., "Piloted Evaluation of Flying-V with Incremental Nonlinear Dynamic Inversion and Envelope Protection," *AIAA SCITECH 2025 Forum*, American Institute of Aeronautics and Astronautics, Reston, Virginia, 2025. https://doi.org/10.2514/6.2025-0973.

[7] Joosten, S., Stroosma, O., Vos, R., and Mulder, M., "Simulator Assessment of the Lateral-Directional Handling Qualities of the Flying-V," *AIAA SCITECH 2023 Forum*, American Institute of Aeronautics and Astronautics, Reston, Virginia, 2023. https://doi.org/10.2514/6.2023-0906, URL https://arc.aiaa.org/doi/10.2514/6.2023-0906.

[8] Torelli, R., Stroosma, O., Vos, R., and Mulder, M., "Piloted Simulator Evaluation of Low-Speed Handling Qualities of the Flying-V," *AIAA SCITECH 2023 Forum*, American Institute of Aeronautics and Astronautics, Reston, Virginia, 2023. https://doi.org/10.2514/6.2023-0907, URL https://arc.aiaa.org/doi/10.2514/6.2023-0907.

[9] Vugts, G., Stroosma, O., Vos, R., and Mulder, M., "Simulator Evaluation of Flightpath-oriented Control Allocation for the Flying-V," *AIAA SCITECH 2023 Forum*, American Institute of Aeronautics and Astronautics, Reston, Virginia, 2023. https://doi.org/10.2514/6.2023-2508, URL https://arc.aiaa.org/doi/10.2514/6.2023-2508.

[10] Boeing Commercial Airplanes, *Statistical Summary of Commercial Jet Airplane Accidents: Worldwide Operations 1959-2022*, The Boeing Company, Seattle, Washington, 2023. URL https://www.boeing.com/content/dam/boeing/boeingdotcom/company/about_bca/pdf/statsum.pdf.

[11] Airbus, *A Statistical Analysis of Commercial Aviation Accidents 1958 - 2024*, AIRBUS S.A.S., X00D17008863 Issue 9., Blagnac, 2025. URL https://accidentstats.airbus.com/wp-content/uploads/2025/02/20241325_A-Statistical-analysis-of-commercial-aviation-accidents-2025-links.pdf.

[12] Zhang, Y., and Jiang, J., "Bibliographical review on reconfigurable fault-tolerant control systems," *Annual Reviews in Control*, Vol. 32, No. 2, 2008, pp. 229–252. https://doi.org/10.1016/j.arcontrol.2008.03.008, URL https://linkinghub.elsevier.com/retrieve/pii/S1367578808000345.

[13] Christopher Edwards, Thomas Lombaerts, and Hafid Smaili, *Fault Tolerant Flight Control*, Lecture Notes in Control and Information Sciences, Vol. 399, Springer Berlin Heidelberg, Berlin, Heidelberg, 2010. https://doi.org/10.1007/978-3-642-11690-2.

[14] Smeur, E. J. J., Chu, Q., and de Croon, G. C. H. E., "Adaptive Incremental Nonlinear Dynamic Inversion for Attitude Control of Micro Air Vehicles," *Journal of Guidance, Control, and Dynamics*, Vol. 39, No. 3, 2016, pp. 450–461. https://doi.org/10.2514/1.G001490.

[15] Kanhai, P., *Adaptive control with Multivariate B-Splines and INDI*, MSc. Thesis, Delft University of Technology, 2022. URL https://resolver.tudelft.nl/uuid:fdd8e2fa-1372-4f79-aa05-6ab152e848e1.

[16] Smit, B., Pollack, T. S., and Kampen, E., "Adaptive Incremental Nonlinear Dynamic Inversion Flight Control for Consistent Handling Qualities," *AIAA Science and Technology Forum and Exposition, AIAA SciTech Forum 2022*, 2022. https://doi.org/10.2514/6.2022-1394.

[17] Atmaca, D., and Van Kampen, E.-J., "Fault Tolerant Control for the Flying-V Using Adaptive Incremental Nonlinear Dynamic Inversion," *AIAA SCITECH 2025 Forum*, American Institute of Aeronautics and Astronautics, Reston, Virginia, 2025. https://doi.org/10.2514/6.2025-0081.

[18] Oosterom, W., and Vos, R., "Conceptual Design of a Flying-V Aircraft Family," *AIAA AVIATION 2022 Forum*, American Institute of Aeronautics and Astronautics, Reston, Virginia, 2022. https://doi.org/10.2514/6.2022-3200, URL https://arc.aiaa.org/doi/10.2514/6.2022-3200.

[19] Asaro, S., and Vos, R., "Synthesis of the Aerodynamic Model of a Flying Wing Aircraft," *AIAA SCITECH 2025 Forum*, American Institute of Aeronautics and Astronautics, Reston, Virginia, 2025. https://doi.org/10.2514/6.2025-0852.

[20] Asaro, S., Atmaca, D., Van Kampen, E.-J., and Vos, R., "Control Surface Allocation Based on Offline Handling Quality Simulations for a Flying Wing Aircraft," *AIAA SCITECH 2025 Forum*, American Institute of Aeronautics and Astronautics, Reston, Virginia, 2025. https://doi.org/10.2514/6.2025-2475.

[21] Van Empelen, S., *Engine Integration of the Flying V*, MSc. Thesis, Delft University of Technology, 2020. URL https://resolver.tudelft.nl/uuid:c519caf8-0eba-4633-a4f9-be37684417a8.

[22] University, C., "BENCHMARK REQUIREMENTS & PERFORMANCE METRICS," Tech. rep., INCEPTION, 2018.

[23] Pollack, T., Theodoulis, S., and van Kampen, E., "Commonalities between robust hybrid incremental nonlinear dynamic inversion and proportional-integral-derivative flight control law design," *Aerospace Science and Technology*, 2024. https://doi.org/10.1016/j.ast.2024.109377.

[24] Grondman, F., Looye, G., Kuchar, R. O., Chu, Q. P., and Van Kampen, E.-J., "Design and Flight Testing of Incremental Nonlinear Dynamic Inversion-based Control Laws for a Passenger Aircraft," *2018 AIAA Guidance, Navigation, and Control Conference*, American Institute of Aeronautics and Astronautics, Reston, Virginia, 2018. https://doi.org/10.2514/6.2018-0385.

[25] Slotine, J. J. E., and Li, W., *Applied Nonlinear Control*, Prentice-Hall, 1991. URL https://api.semanticscholar.org/CorpusID:106519536.

[26] Van 't Veld, R. C., *Incremental Nonlinear Dynamic Inversion Flight Control*, MSc. Thesis, Delft University of Technology, 2016. URL https://resolver.tudelft.nl/uuid:f85a9c88-7bdb-42cd-a01c-aa85251d365c.

[27] Wang, S., *Incremental sliding mode flight control*, Doctoral Thesis, Delft University of Technology, 2019. URL https://resolver.tudelft.nl/uuid:c8259a08-bbee-4af0-b570-1350a2dd8d89.

[28] Acquatella, P. J., *Robust Nonlinear Spacecraft Attitude Control an Incremental Backstepping approach*, MSc. Thesis, Delft University of Technology, 2011. URL https://resolver.tudelft.nl/uuid:a56090a3-bbce-404b-8e4b-d0e9050b518a.

[29] Acquatella Bustillo, P., *Robust nonlinear attitude control of aerospace vehicles: An incremental nonlinear control approach*, Doctoral Thesis, Delft University of Technology, 2020. https://doi.org/10.4233/uuid:99d82992-080c-4c5d-8d40-4e62e62285c0.

[30] Durham, W., Bordignon, K. A., and Beck, R., *Aircraft Control Allocation*, Wiley, 2016. https://doi.org/10.1002/9781118827789.

[31] Luo, F., Zhang, J., and Jiang, B., "Robustness Analysis of Two Advanced Flight Control Laws: NDI and INDI," *Lecture Notes in Electrical Engineering*, Vol. 821 LNEE, Springer Science and Business Media Deutschland GmbH, 2022, pp. 660–668. https://doi.org/10.1007/978-981-16-7423-5{_}64.

[32] Pollack, T., and Van Kampen, E.-J., "Robust Stability and Performance Analysis of Incremental Dynamic Inversion-based Flight Control Laws," *AIAA SCITECH 2022 Forum*, American Institute of Aeronautics and Astronautics, Reston, Virginia, 2022. https://doi.org/10.2514/6.2022-1395.

[33] Lombaerts, T. J. J., *Fault Tolerant Flight Control*, Doctoral Thesis, Delft University of Technology, 2010. URL https://resolver.tudelft.nl/uuid:538b0174-fe84-43af-954d-02f256b2ec50.

[34] Campbell, S., Nguyen, N., Kaneshige, J., and Krishnakumar, K., "Parameter Estimation for a Hybrid Adaptive Flight Controller," *AIAA Infotech@Aerospace Conference*, American Institute of Aeronautics and Astronautics, Seattle, Washington, 2009. https://doi.org/10.2514/6.2009-1803.

[35] Fortescue, T., Kershenbaum, L., and Ydstie, B., "Implementation of self-tuning regulators with variable forgetting factors," *Automatica*, Vol. 17, No. 6, 1981, pp. 831–835. https://doi.org/10.1016/0005-1098(81)90070-4.

[36] Stougie, J., *Incremental Nonlinear Dynamic Inversion Control with Flight Envelope Protection for the Flying-V*, MSc. Thesis, Delft University of Technology, 2022. URL https://resolver.tudelft.nl/uuid:5d0a883c-bf58-4507-b688-6abccdca4842.

[37] Anonymous, "Flying Qualities of Piloted Aircraft," , 1990. MIL-STD-1797A, Department of Defense Interface Standard, originally issued January 30, 1990.

[38] Anonymous, "Flight Control Design–Best Practices," Tech. rep., NATO Research and Technology Organization (RTO), 2000.

[39] Cook, M. V., *Flight Dynamics Principles: A Linear Systems Approach to Aircraft Stability and Control*, Elsevier, 2012. https://doi.org/10.1016/C2010-0-65889-5.

[40] Anonymous, "Flight Control Systems – Design, Installation, and Test of Piloted Aircraft," , 2008. MIL-DTL-9490E, Department of Defense Detail Specification, issued April 22, 2008.

[41] Mitchell, D. G., and Hoh, R. H., "Low-Order Approaches to High-Order Systems: Problems and Promises," *Journal of Guidance, Control, and Dynamics*, Vol. 5, No. 5, 1982, pp. 482–489. https://doi.org/10.2514/3.56195.

[42] Mitchell, D. G., Klyde, D. H., Hoh, R. H., and Aponso, B. L., "Proposed Incorporation of Mission-Oriented Flying Qualities into MIL-STD-1797A," Technical Report WL-TR-94-3162, Wright Laboratory, Wright-Patterson Air Force Base, OH, USA, October 1994.